Supporting information for

Efficient degradation of organic pollutants with sewage sludge support and *in-situ* doped TiO_2 under visible light irradiation conditions

Shi-Jie Yuan, Xiao-Wei Li, Xiao-Hu Dai*

State Key Laboratory of Pollution Control and Resource Reuse, College of Environmental Science and Engineering, Tongji University, Shanghai, 200092, China

***Corresponding author:**

Prof. Xiao-Hu Dai, Phone: +86-21-65986297; Fax: +86-21-65983602; E-mail: daixiaohu@tongji.edu.cn

This Supporting Information contains 16-page document, one table, seven figures, including this cover page.

Experimental

Characterization of the as-synthesized catalysts. X-ray diffraction (XRD; X' Pert PRO, Philips Co., The Netherlands) and scanning electron microscopy (SEM; FEI Co., The Netherlands) were used to characterize the crystal structure and image the morphology of the as-synthesized catalysts, respectively. The surface area analysis was carried out using the Brunauer-Emmett-Teller (BET) method with a Builder 4200 instrument (Tristar II 3020M, Micromeritics Co., USA). The functional groups of the as-prepared catalysts were determined by Fourier transform infrared (FTIR) spectra recorded with a VERTEX 70 FT-IR (Bruker Co., Germany) equipped with a deuterium triglycine sulfate (DTGS) detector. The UV-vis diffuse reflective spectra were collected using a DUV-3700 spectrometer (DUV-3700, Shimadzu Co., Japan) with $BaSO_4$ as the reference. The electronic environment of the catalyst was investigated using X-ray photoelectron spectroscopy (XPS, PHI-5000C, Perkin Elmer), and the composition of the catalysts was measured via inductively coupled plasma spectrometry (ICP, Agilent 720ES, USA) after total digestion in a microwave using a mixture of HNO_3+HCl+HF. The C, H, and N contents of the materials were determined by a Vario EL III Elemental Analyze (vario EL Ⅲ, GmbH, Germany). Electron paramagnetic resonance (EPR) spectroscopy were recorded at 298 K using a Bruker EMX-8/2.7C electron paramagnetic resonance spectrometer to study the material for valuable information about the lattice site. Electron spin resonance (ESR) signals of hydroxyl radical ($OH^{\bullet}$) radicals trapped by 5,5-dimethyl-1-pyrroline N-

oxide (DMPO) were recorded at ambient temperature on a JEOL JES-FA200 X-band spectrometer (9.072 GHz) (JEOL Co. Japan) with a 500-W Xe-arc lamp as the light source.

Photocatalytic organic pollutant degradation. A 30-W low-pressure mercury lamp was also used as the UV light source for the photocatalytic *p*-nitrophenol degradation under UV light irradiation conditions and fixed next to the cylinder. Outdoor photocatalytic reactions under solar light irradiation were also carried out during day time between 9 a.m. and 2 p.m. on 21 August 2014, in Shanghai, China (31.29 °N, 121.50 °E). In a typical run, 0.15 g of the as-synthesized catalyst was dispersed into the quartz glass cylinder, except for the control test in which no catalyst was added. The suspension was stirred in the dark for 1 hour to disperse the catalyst and reach the adsorption equilibrium (Fig. S1B). At the end of this initial period, the first sample was taken to determine the initial concentration C_0. The lamp was then turned on to initiate the degradation reaction. During the reaction, solution samples were taken at given time intervals and centrifuged at 4^{o}C to immediately remove any catalyst particles. The stability and recyclability of the as-synthesized catalyst were evaluated by recycling and reusing the catalyst several times under the same conditions. The degradation of *p*-nitrophenol in the presence of various scavengers in solution under the same conditions was also investigated.

The photoelectric conversion property of the photocatalyst materials were evaluated by short-circuit photocurrent using a potentiostat (660C, CH Instruments, Inc., USA) in a conventional three-electrode system assembled with an Ag/AgCl

reference electrode, a Pt coil counter electrode, and a 500 W Xe arc lamp (PLS-SXE500, Beijing Trusttech Co., China) as the light source. The electrolyte solution used is composed of 0.1 M Na_2SO_4 and 35 mg/l *p*-nitrophenol. The photoelectrodes were prepared by painting SS-Ti-700 and TiO_2 (P25) on ITO electrode respectively.

Results and Discussion

FTIR spectra. FTIR spectra were used to characterize the chemical bonds and functional groups on the catalyst surfaces (Fig. S2D). Comparing the SS-Ti-700 and TiO_2 curves, some new peaks, such as the characteristic asymmetric stretching vibrations of the Si-O-Si (1,080 cm^{-1}) and the shoulder at 952 cm^{-1}, corresponding to a Si-O-Ti linkage, were observed[S1]. These features clearly indicate the formation of Si-O-Ti binding between the SiO_2 in the sewage sludge and the loaded TiO_2 nanoparticles in the as-synthesized SS-Ti-700. No obvious Fe-associated peaks were observed in the SS-Ti-700 spectra, which may have overlapped with the broad high intensity Ti-O-Ti peaks in the fingerprint region.

During a typical *p*-nitrophenol degradation process under UV light irradiation conditions, the rapid decrease of the peak intensity at 317 nm, which decreased by 87.40% within 30 min, clearly evidenced its continuous effective degradation (Fig. S5A). The SS-Ti-700 had a pseudo-first-order degradation rate constant of 0.0756±0.0021 min^{-1}, significantly higher than that for the commercial P25 (0.0211±0.0029 min^{-1}) (Fig. S5B). A removal efficiency of 87.77±1.13% was achieved for the SS-Ti-700 under solar light irradiation conditions, much higher than

that for the commercial P25 (32.82±1.57%) (Fig. S5C). These results indicate the effectively catalytic ability of the as-synthesized SS-Ti-700 both under UV and solar light irradiation conditions.

Different from the low increased current at +0.5 V, the sharp increase of reverse currents for both the *I-V* curves of the SS-Ti-700 and TiO_2 were observed at -0.5 V, suggesting a strong intrinsic nanoscale effect (Fig. S7A). The *I-V* curve of the SS-Ti-700 exhibited typical characteristic asymmetric behavior, confirmed the formation of schottky barrier between TiO_2 and the doped metal ions[S2]. As a benefit from the schottky barrier, photogenerated electrons would transfer from TiO_2 to the doped metal ions, and thereby expediting the separation of photogenerated charge carriers. The photocurrent responsive under light irradiation conditions confirmed the photoelectric conversion property of the as-synthesized SS-Ti-700 (Fig. S7B). Compared to the TiO_2 (Fig. S7C), the higher photocurrent response of SS-Ti-700 indicated the higher photoelectron separation and transfer efficiency, which is beneficial for improving the efficiency of the photocatalytic process. This further confirmed that the metal-ion doping, which is responsible for the visible light activity of the as-synthesized SS-Ti-700, can also inhibit the recombination of the photogenerated electrons and holes by increasing the charge separation and thus the efficiency of the photocatalytic process. It was observed that the lifetimes of the photogenerated electron in the Fe-doped TiO_2 were increased to 50 ms, whereas undoped TiO_2 had a shorter lifetime of <200 μs[S3]. Therefore the doped metal-ions, major Fe^{3+}, can provide a shallow trap for photo-generated electron and hole, and

consequently resulting in a markedly higher photocatalytic activity of the as-synthesized catalyst under both UV and solar light irradiation conditions (Fig. S5).

The identified intermediates in the *p*-nitrophenol degradation process indicated that the pathway of $OH^{\bullet}$ react with *p*-nitrophenol seems to occur in two steps (Fig. S6). For one way, the $OH^{\bullet}$ would attack the $NO_2^{\bullet}$ group due to the relatively long length of C-N bond[S4]. The $OH^{\bullet}$ would add on the aromatic ring with benzoquinone and hydroquinone formation. The removed $NO_2^{\bullet}$ with electron transfers can be reduced to generate NO_2^- which is finally oxidized to be NO_3^- by oxygen dissolved in the solution[S5]. The other is starting from the electrophilic addition between the $OH^{\bullet}$ and the *p*-nitrophenol, with the position at the third of the benzene ring as the strong electron withdrawing ability of the $NO_2^{\bullet}$ group. *p*-Nitrocatechol and 1,2,4-benzenetriol were produced with electron transfers and detected as expect[S6] (Fig. S4). These primary intermediates would react with the $OH^{\bullet}$ further, leading to benzene ring cleavage and mineralization of *p*-nitrophenol, as being confirmed by the decreased TOC of the solution.

Differ from the micromolecule organics, such as urea[S7], melamine borate[S8], tetrabutylammonium hydroxide[S9], and glucose[S10] that can be used as the precursor to obtain C-doped TiO_2, the carbon in the sewage sludge is mainly in the form of biomacromolecules, such as polysaccharides, proteins, fats, and cellulose. These biomacromolecules might not act as the suitable C precursor to obtain C-doped TiO_2 during the synthesized process. It is suggest that the negligible peak at 282 eV of the C1s spectra corresponding to the Ti-C specie[S11] was probability attributed to the

binding between the scaffold templates and TiO_2 (Fig. S3A), instead of C in the TiO_2 lattice. Thus the C in the sewage sludge, mainly in the form of biomacromolecules and will carbonize or combust during the synthesized process, may act as the scaffold templates instead of a precursor to obtain C-doped TiO_2. The low level of C content (0.38%) in the SS-Ti-700 further confirmed this conclusion (Table 1). The Al, Ca, Mg and Na content of the as-synthesized catalyst might be assigned to the undissolved content in the sewage sludge acting as the scaffold templates. Even partially of them could act as the dopants, the other detected metals in the SS-Ti-700, $A1^{3+}$ and Mg^{2+} for instance, which have a closed-shell electronic configuration and makes electron (or hole) trapping unfavorable, may hardly have any effect on the observed photoreactivity[S3].

References

S1 A.N. Murashkevich, A.S. Lavitskaya, T.I. Barannikova, and I.M. Zharskii, *J. Appl. Spectrosc*., 2008, **75**, 730-734.

S2 H. Chen, S. Chen, X. Quan, H.T. Yu, H.M. Zhao, and Y.B. Zhang, *J. Phys. Chem. C*., 2008, **112**, 9285-9290.

S3 W. Choi, A. Termin, and M.R. Hoffmann, *J. Phys. Chem*., 1994, **98**, 13669-13679.

S4 Q.Z. Dai, L.C. Lei, and X.W. Zhang, *Sep. Purif. Technol*., 2008, **61**, 123-129.

S5 A. Di Paola, V. Augugliaro, L. Palmisano, G. Pantaleo, and E. Savinov, *J.*

Photochem. Photobiol. A, 2003, **155**, 207-214.

S6 L. Yang, S. Luo, Y. Li, Y. Xiao, Q. Kang, and Q. Cai, *Environ. Sci. Technol*., 2010, **44**, 7641-7646.

S7 T. Tachikawa, S. Tojo, K. Kawai, M. Endo, M. Fujitsuka, T. Ohno, K. Nishijima, Z. Miyamoto, and T. Majima, *J. Phys. Chem. B*, 2004, **108**, 19299-19306.

S8 E.M. Neville, M.J. Mattle, D. Loughrey, B. Rajeshi, M. Rahman, J.M. Don MacElroy, J.A. Sullivan, and K.R. Thampi, *J. Phys. Chem. C*, 2012, **116**, 16511-16521.

S9 D.M. Chen, Z.Y. Jiang, J.Q. Geng, Q. Wang, and D. Yang, *Ind. Eng. Chem. Res*., 2007, **46**, 2741-2746.

S10 J. Zhong, F. Chen, and J.L. Zhang, *J. Phys. Chem. C*, 2010, **114**, 933-939.

S11 D.E. Gu, Y. Lu, B.C. Yang, and Y.D. Hu, *Chem. Commun*., 2008, **21**, 2453-2455.

Table S1. Textural Properties of the as-synthesized catalysts.

	BET surface area (m^2/g)	total pore volume (cm^3/g)	average pore size [a] (nm)
TiO_2	27.09	0.11	25.59
SS-700	10.52	0.04	22.21
SS-Ti-700	35.46	0.10	16.12

[a] Calculated from the Barrett-Joyner-Halenda (BJH) equation using the desorption isotherm.

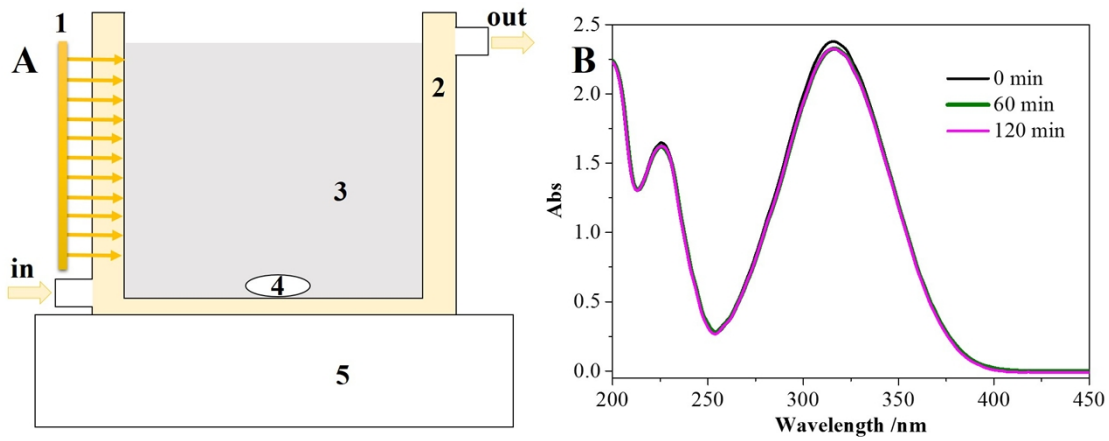

Figure S1. The schematic presentation of the experimental setup (A) and a typical UV-vis spectra of *p*-nitrophenol during the adsorption equilibrium process (B). (1) Philips 100-W halogen lamp; (2) the quartz glass cooling jacket filled with 2 M $NaNO_2$ acting as the cutoff filter; (3) the quartz glass cylinder; (4) stirrer and (5) magnetic stirrer.

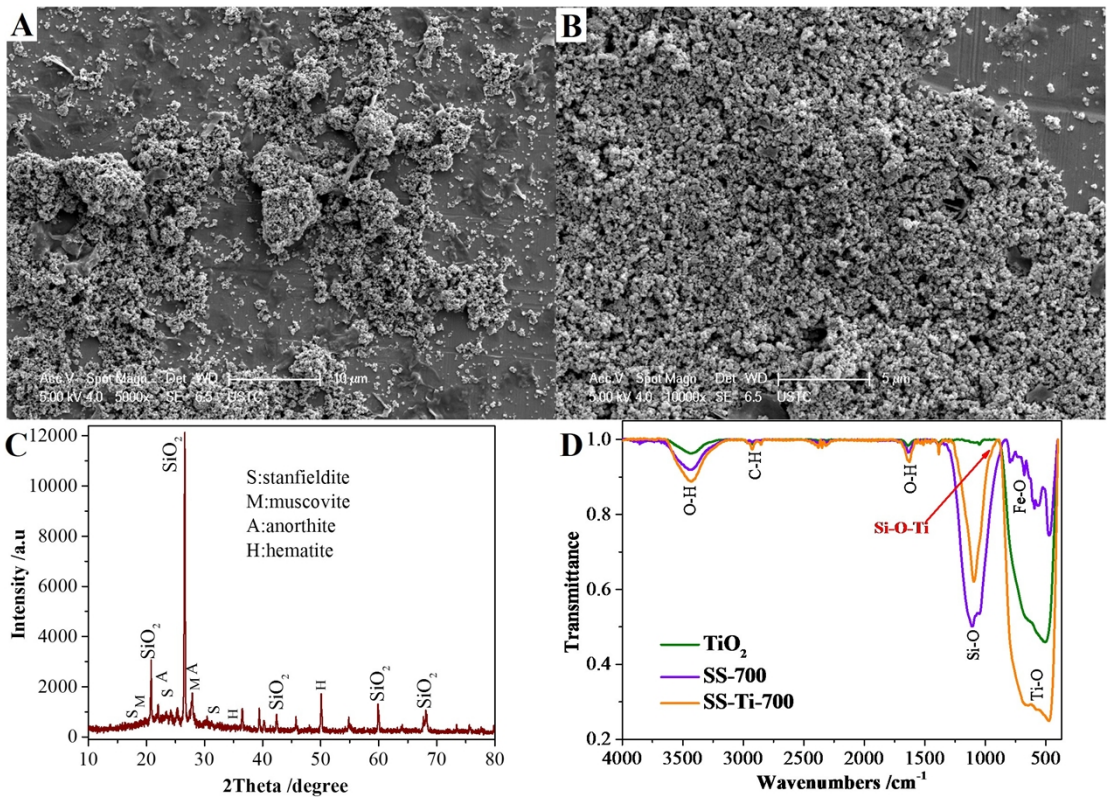

Figure S2. SEM images of the as-prepared SS-Ti-700 in the low magnification (A and B). XRD of the control sample SS-0-700, which was obtained by the same synthesized procedure of catalyst with no $TiOSO_4 \bullet 2H_2O$ added (C). FTIR spectra of the SS-700, TiO_2, and as-synthesized SS-Ti-700 (D).

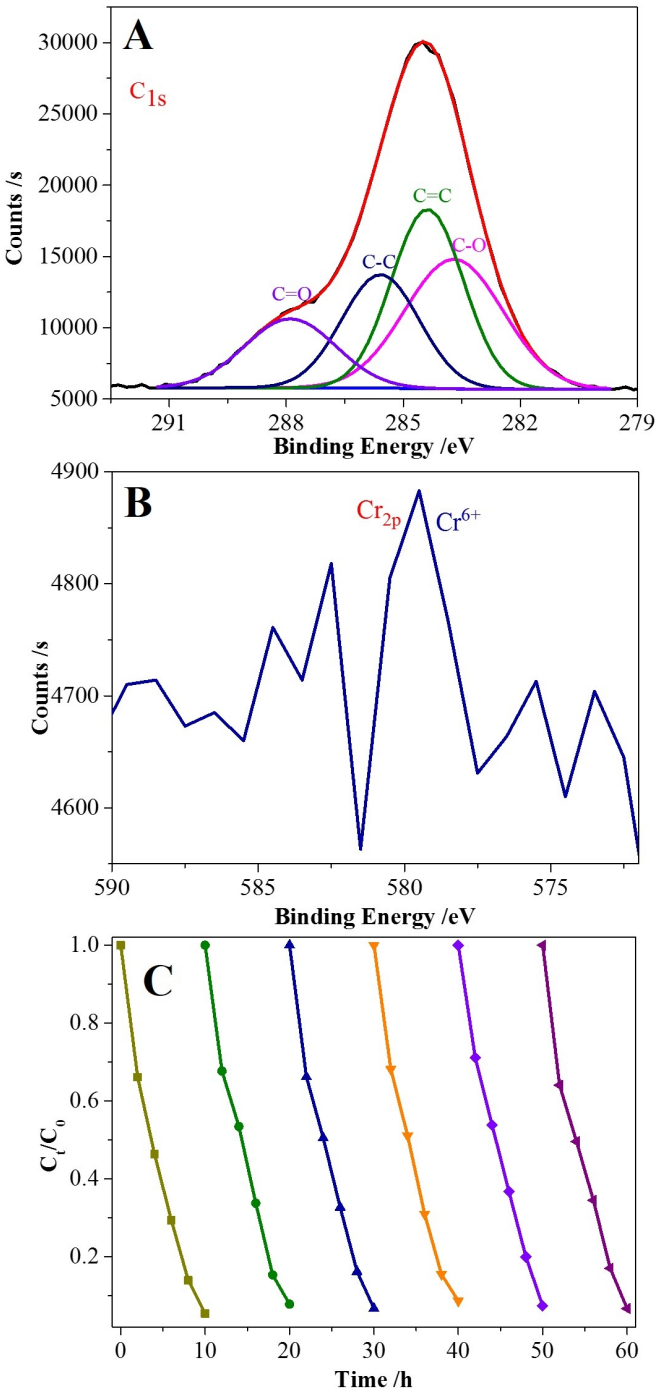

Figure S3. X-ray photoelectron spectra of the C 1s (A) and Cr 2p (B) from the catalyst SS-Ti-700 is shown respectively. Cyclic degradation in repetitive *p*-nitrophenol degradation under visible light irradiation conditions (C).

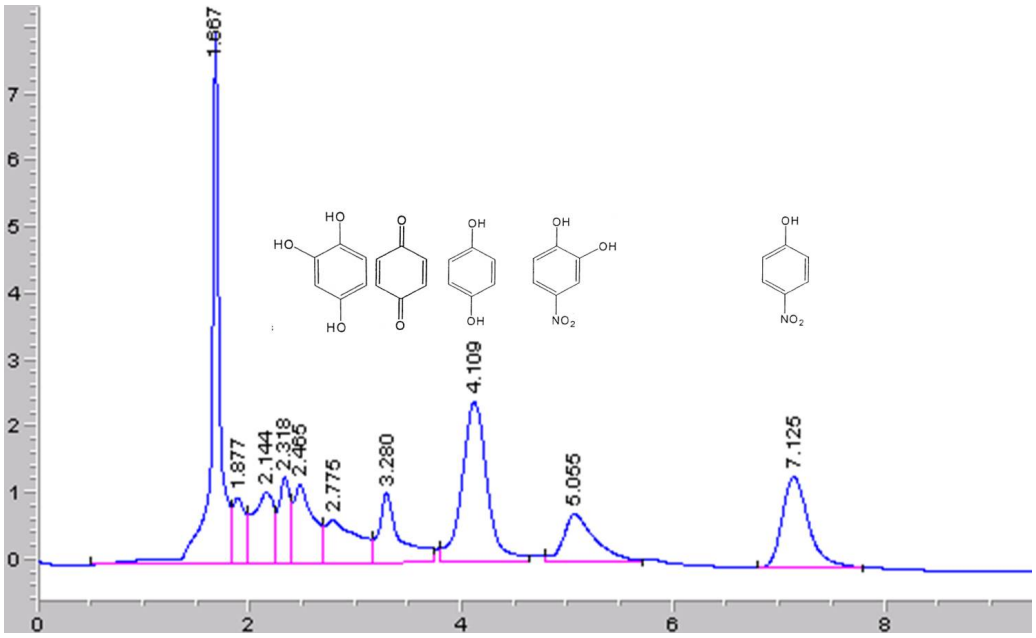

Figure S4. Intermediate products during the *p*-nitrophenol degradation process.

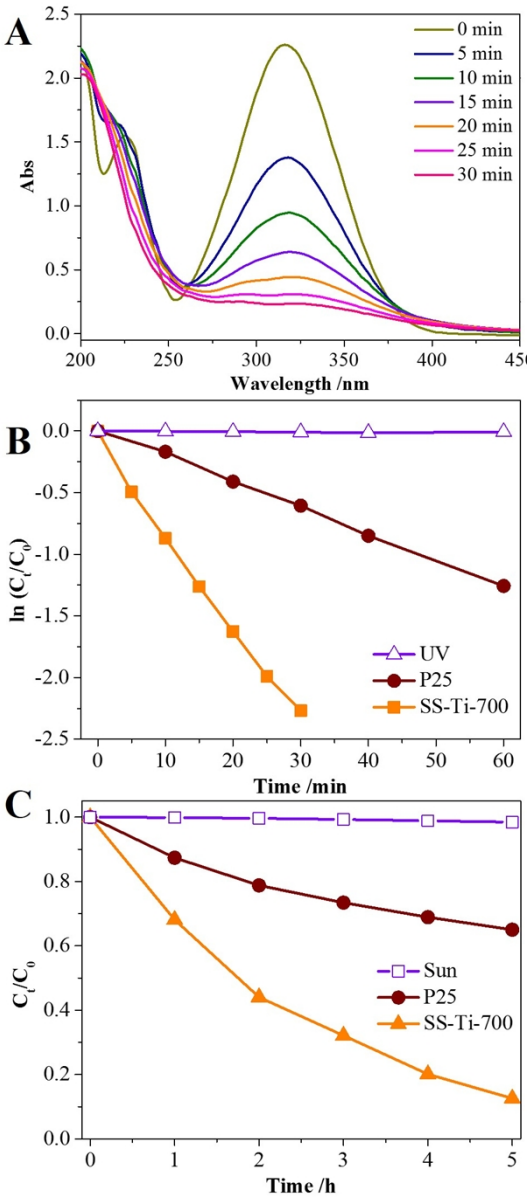

Figure S5. Photocatalytic activity of the catalysts under UV and solar light irradiation conditions. (A) UV-vis spectra of *p*-nitrophenol in a typical degradation process under UV irradiation conditions. (B) The relative concentration profiles of *p*-nitrophenol during a typical degradation processes under UV light irradiation conditions. (C) The relative concentration profiles of *p*-nitrophenol during typical degradation processes under solar light irradiation conditions during day time between 9 a.m. and 2 p.m. on 21 August 2014, in Shanghai, China (31.29 °N, 121.50 °E).

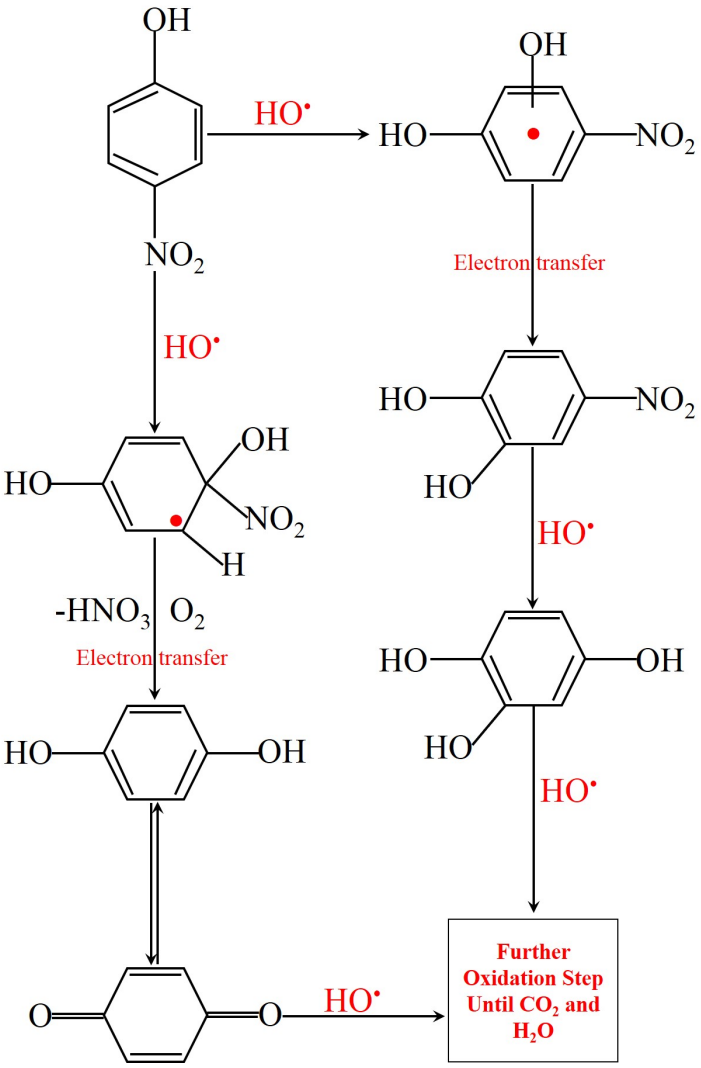

Figure S6. Proposed pathway for the photocatalytic *p*-nitrophenol degradation and intermediates production.

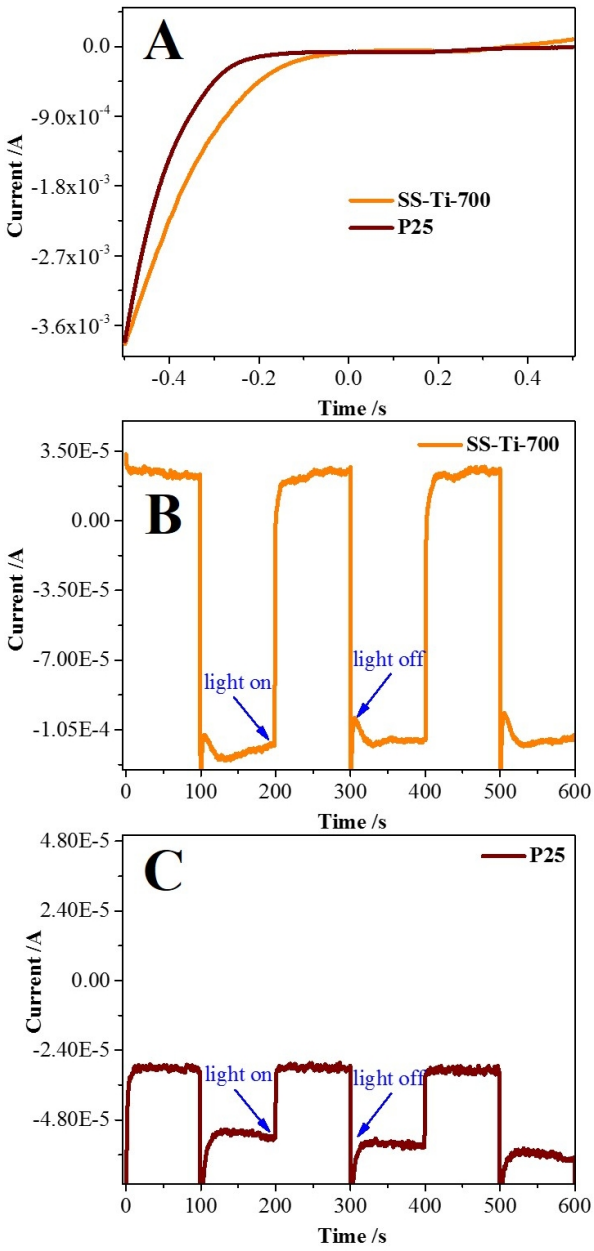

Figure S7. The current-voltage (*I-V*) curves of SS-Ti-700 and TiO_2 in the dark (A). The short-circuit photocurrents of SS-Ti-700 (B) and TiO_2 (C) at +0.20 V (versus Ag/AgCl) under light irradiation conditions.